Monitoring the land subsidence with persistent scatterer interferometry in Nansha District, Guangdong, China

Minsi Ao · Changcheng Wang · Rongan Xie · Xingqing Zhang · Jun Hu · Yanan Du · Zhiwei Li · Jianjun Zhu · Wujiao Dai · Cuilin Kuang

Abstract Nansha District in Guangzhou, south China, as a well-known rapid urbanization area, is characterized by the widely distributed soft soil prone to land subsidence. Accurate monitoring of surface deformation plays a significant role for the hazard prevention and mitigation. In this study, 21 high-resolution TerraSAR-X satellite images acquired from February 2012 to August 2013 are processed with the persistent scatterer interferometry (PSI) technology to detect and reveal the land subsiding characteristics of Nansha District. Based on the comparisons among the PSI, the GPS measurements, and the civil construction process, the land subsiding characteristics are discussed. The difference between PSI and GPS velocity rates on the line of sight direction is less than 3.61 mm/year, showing fairly consistent agreement. Meanwhile, the PSI results show that the Nansha Automobile Industrial Area, Tongxin Industrial Area, Xinan Industrial Area, Nanheng, and Dugang of Sanjiao town in Zhongshan City were stable, where the subsidence velocities were less than −5 mm/year. The moderate subsidence, whose velocities ranged from −20 to −5 mm/year, mainly occured in the Dayuancun village and Gaoping village of Sanjiao town in Zhongshan City. The severely subsiding areas, where the velocities are more than −20 mm/year, were detected in Nansha Export Processing Zone and Minzhong town in Zhongshan City. For the primary roads and bridges, the newly built bridges, such as Hengli Flyover and southern side of Fuzhou Bridges, were suffering a subsidence velocity from −10 to −15 mm/year. On the contrary, the old roads and bridges turned out to be stable, for instance, the Nanshagang Expressway, Hongqili and Lixinsha Bridges. The civil engineering documents and other related materials show that most of the subsidence took

M. Ao · C. Wang (✉) · Y. Du · Z. Li · J. Zhu · W. Dai · C. Kuang
School of Geoscience and Info-physics, Central South University, Lushannan Road No. 932, Changsha, China
e-mail: wangchangcheng@csu.edu.cn

R. Xie · X. Zhang
Guangdong Institute of Surveying and Mapping of Geology, Xinjie Avenue No. 50, Guangzhou, China

J. Hu
Department of Land Surveying and Geo-Informatics, The Hong Kong Polytechnic University, Kowloon, Hongkong, China

place within the rational post-construction period. However, the subsidence in and around self-constructed substandard houses in the countryside are rather severe due to the lack of sufficient soft soil foundation treatment.

1 Introduction

The Nansha District in Guangzhou, south China, is well known for its rapid urbanization process as well as for the widely distributed soft soil, which is prone to geological hazards. Located in the west bank of the intersection of the Pearl River and Lindingyang Estuary, south of Guangzhou City, the area of Nansha is about 803 km^2. It covers the regions of Nansha, Zhujiangjie, Huangge, Hengli, Wanqingsha and Longxuedao. In 2005, the Nansha District became the National Economic and Technical Development Zone. Subsequently, it has been experiencing a rapid full-scale development under the strong support from the government. For instance, from 2007 to 2011, the resident population increased from 192,000 to 736,000 and the regional gross domestic product (GDP) increased from 30.57 to 81.3 billion Chinese Yuan. During this period, the ecological environment is under huge pressure due to the mass construction. The widely distributed soft soil gradually turned out to be geological environment hazards such as land subsidence and collapse. However, almost all the monitoring on land surface subsidence is mainly organized by civil construction projects. The dominant monitoring methods were using the total station, leveling and GPS stations, which are sparsely distributed. It is difficult to reveal the overall land subsidence of Nansha District, which is characterized by large-scale and high spatial resolution. Accordingly, the hazard prevention and mitigation work were also limited.

Synthetic aperture radar (SAR) remote sensing images have been widely used in geological and environment monitoring applications (Schmullius and Evans 1997; Ouchi 2013; Cigna et al. 2011, 2012). The detection of the surface deformation and subsidence is also possible through the phase observations in two SAR images (Gens and Van Genderen 1996; Massonnet and Feigl 1998). In the conventional SAR interferometry, it computes the interference pattern caused by phase difference between two images with similar look angles. With correction of topographic and orbital contributions, assuming that atmospheric effects are negligible or mitigating them through estimation or external observations, the resulting interferogram could map the deformation between acquisition pairs. The main limitations of the conventional InSAR are temporal, spatial decorrelation, and atmospheric effects. To solve these problems, Ferretti et al. (2000, 2001) proposed the persistent scatterer interferometry (PSI). The basic idea of PSI is to reduce the decorrelation and atmospheric effects through a group of scatterers with stable radar backscattering characteristics. Then the sub-millimetric deformation could be detected on these scatterers that usually correspond to the stable natural or man-made reflectors, such as building or large rock (Kampes 2006; Wegmuller et al. 2010; Bianchini et al. 2012, 2013). PSI technology has been successfully applied in wide urbanized areas such as Las Vegas, Los Angeles, Mexico City, Lisbon, Seattle, Hongkong, Beijing, and Shanghai (Amelung et al. 1999; Hoffmann et al. 2001; Bawden et al. 2001; Zhang et al. 2012; Cabral-Cano

et al. 2008; López-Quiroz et al. 2009; Heleno et al. 2011; Finnegan et al. 2008; Perissin and Wang 2011; and Chen et al. 2011, 2013).

The classic PSI method improves the accuracy of deformation detection. However, the PS is not easy to be found in rural areas due to the weak reflected amplitude. Based on previous studies, some modified or more sophisticated methods were proposed. Some aim at the distributed scatterer, which are widely distributed, but do not show enough reflection stability, such as SqueeSAR (Ferretti et al. 2011). It achieves good results in rural area where there are a large number of homogeneous scatterers. Another popular method is presented by Hooper (2004), the StaMPS/MTI (Stanford Method for Persistent Scatterers/Multi-Temporal InSAR). Instead of making the use of amplitude, it uses the stability of phase observations to define and extract the PSs. Therefore, it does not require a large number of homogeneous scatterers. The process makes the corrections first to facilitate the coherence among multi-temporal images and then estimates the deformation parameters. The case studies from Taiwan, Staufen, Kyrgyzstan, Czech, and some active volcano-affected places (Chang et al. 2010; Lubitz et al. 2011; Motagh et al. 2013; Milan and Eva 2010; Hooper et al. 2007, 2008) show that the StaMPS can effectively improve density of PSs and achieves better results in the suburban, urbanizing and rural areas. Through the monitoring of the land subsidence of these areas, it helps understand the conditions of geological processes and find the potential hazards and then provide useful knowledge for taking the suitable measures to avoid or mitigate the losses.

Considering the two facts that this area is urbanizing and well vegetated, the potential land subsidence would be caused by mass civil constructions. Three problems should be addressed during the land subsidence monitoring. The first problem is the limited number of PSs due to the weak coherence from vegetation. The second one is that the spatial resolution issue. The spatial resolution needs to be high enough for the scale of civil constructions. The final problem is that the temporal resolution is also required to be fit for high deformation velocity after civil construction. To solve these problems, 21 TerraSAR-X images, with 3-m spatial resolution and 22-day repeating period, are collected and processed by the StaMPS/MTI algorithm in the study area.

2 Data collection and processing

2.1 Area of interest and data collection

Nansha District, located in the estuary of Pearl River, is not only the geographic center of the Pearl River delta, but also an important traffic hub and harbor for the nearby cities. Figure 1a shows the location of the area of interest (AOI). From the geo-structural point of view, the area belongs to the northeastern part of Wanqingsha fault depression. The center of Wanqingsha fault is the Zhongshan Depression. Shiqiao-Xinhui, Shanwan, Wugui-shanbeilu, and Xijiang fractures are distributed in the northwest, northeast, southeast, and southwest direction, respectively. The seismic activity in this region is rare. In AOI, the earthquakes stronger than 4M.s have not been observed in history (http://www.csi.ac.cn/manage/eqDown/html/gdnew_2.htm). The quaternary dating observation shows the tectonic movement in this region is dominated by ground subsidence (Song et al. 2003; Yao et al. 2008). Furthermore, the subsidence velocity in the western portion of the area is slightly slower than that in the east. The maximum quaternary vertical tectonic movement velocity is ranged from −1 to −2 mm/year, which is estimated from the data of Quaternary deposits in fossil delta. (Chen et al. 2011). From the hydrogeological point of view, the

surface of this region is mainly covered by quaternary loose rock. The sediment with the thickness of about 76 m is primarily composed of sand, clay, and their mixture. The characteristic of the groundwater is principally the Cl type, which is one of the typical salt water (Zheng and Liu 2006; Wang and Liu 2011). In addition, the recharge of ground water is relatively rich and stable. It mainly comes from the precipitation. Since it is unsuitable for drinking, the groundwater is not overexploited in the study area. Generally, the level of groundwater is <3 m, and its fluctuation is very weak (Xu et al. 2009; Wu et al. 2011).

It can be found that most of the land in AOI is used for agriculture, and the elevation is approximately equal to the sea level. Most area of the AOI is flat except a small region in north, which is a forest park called Huangshanlu. The center of the AOI is Wanqingsha town, which is the largest town in Nansha District, with an area of about 271 km². It is surrounded by three canals, i.e., Xiahengli, Shanghengli, and Jiaomen Canals. Region A in Fig. 1b is the town center with dense population. It includes the residential land, wetland park, administrative, and business departments. It is worthy to note that regions E and F named as Tongxin and Xinan, respectively, are in the western part of Wanqingsha town, next to the Hongqili Canal. These two areas are planned for warehouse and industrial zone by the government. The Hengli town, (region B in Fig. 1b), is adjacent to Wanqingsha in the north and is located in the center of three canals, the Xiahengli, Jiaomen, and Shanghengli Canals (in north, not denoted in Fig. 1b). It is planned to be the commercial and logistics zone due to its convenient transportation. The similar situations can be found in the Nansha Export Processing Zone in central Wanqingsha Town, (region D in Fig. 1b). Nanheng, (region C in Fig. 1b), is mainly constructed for the scientific research and education purpose. On the southwest of Hongqili Canal, they are the Gaoping village and Minzhong town of Zhongshan City. Due to the similar geological environments, they also suffer from the comparable types of land subsidence. Meanwhile, the rich external observations in this region would be helpful for the validation of the PSI results. Overall, from the discussion on regional tectonic geological, hydro geological condition, and the development plans, the main cause of the land subsidence is the rapid industrial construction and the widely distributed soft soil property. Therefore, the discussion of the deformation characteristic in the paper will be closely associating with the soft soil foundation treatment designs and procedures.

In this study, 21 scenes of high-resolution TerraSAR-X satellite descending images are collected from February 2012 to August 2013, (Table 1). All the images are acquired in StripMap mode with a 3-m resolution on both azimuth and range directions. As shown in Table 1, the total monitoring period is 451 days in this study. The mean repetition period is about 21.5 days. For the Doppler centroid frequencies of images, the mean is 1.55 Hz and standard deviation is 22.45 Hz. Compared with the previous intermediate or low-resolution satellite, the small deviation of the Doppler centroid frequencies can effectively improve the coherence of interferograms.

2.2 Data processing

During the master image selection, on one hand, the temporal, perpendicular baselines and backscattering feature are considered. On the other hand, the image in winter is preferred because the weather is dry and the atmospheric effects would be small. Finally, the image acquired in 2013/01/16 is selected as the master image.

The temporal baselines of all the 20 interferograms are not more than 330 days, and the largest perpendicular spatial baseline is about 188.9 m (Fig. 2). After precise registration,
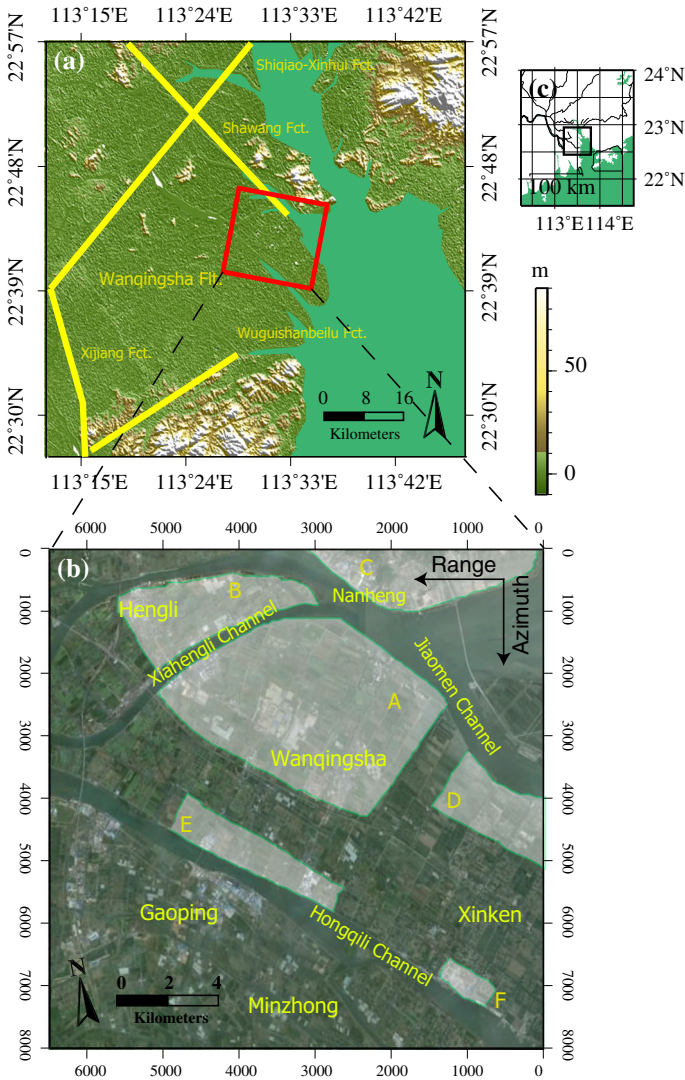
Fig. 1 **a** Location of the area of interest (AOI). The *red rectangle* represents the AOI, and *yellow lines* represent the primary surrounded geological fractures. **b** Optical satellite image of the AOI in radar coordinate system. *Letters A* to *F* represent the main regions considered in the study. **c** The *black rectangle* represents the location of area covered by (**a**).

interferogram generation, and topographic contributions flattening and geocoding, PS processing could be started. According to the StaMPS/MTI algorithm, the model of phase observation is as Eq. (1),

$$\phi_{x,i} = W\big\{ \phi_{D,x,i} + \phi_{A,x,i} + \Delta\phi_{L,x,i} + \Delta\phi_{S,x,i} + \phi_{N,x,i} \big\} \tag{1}$$

where the $\phi_{x,i}$ is the wrapped phase observation for pixel x in interferogram i. The $W\{\}$ is the wrapping operator. The $\phi_{D,x,i}$ and $\phi_{A,x,i}$ represent the deformation and atmospheric

Table 1 The date and Doppler centroid frequency (f_{DC}) of the TerraSAR-X images

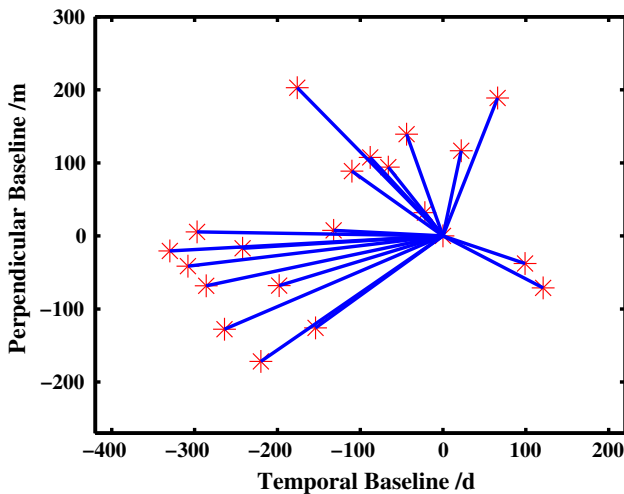| No.	Date	f_{DC} (Hz)	No.	Date	f_{DC} (Hz)
1	2012/02/21	8.09	12	2012/11/11	−8.89
2	2012/03/14	29.01	13	2012/12/03	10.69
3	2012/03/25	38.70	14	2012/12/25	10.33
4	2012/04/05	−5.22	15	2013/01/16	−39.32
5	2012/04/27	−6.26	16	2013/02/07	−27.97
6	2012/05/19	−2.30	17	2013/03/23	−8.50
7	2012/06/10	31.63	18	2013/04/25	−18.10
8	2012/07/02	−38.32	19	2013/05/17	34.11
9	2012/09/06	−8.82	20	2013/06/08	−5.42
10	2012/09/28	27.52	21	2013/07/22	0.144
11	2012/10/20	11.55	–	–	–

Fig. 2 The temporal and perpendicular baselines

components. The $\Delta\phi_{L,x,i}$ is the residual look angle error. It is the error caused by the phase change on look angle. It mainly consists of the residual DEM error and the contribution due to the difference between the positions of the dominant scatter and the center of ground pixel. The $\Delta\phi_{S,x,i}$ and $\phi_{N,x,i}$ are, respectively, the residual satellite orbital error and random noises. One of the most important modification of the StaMPS procedure is the definition and selection of PS.

It defines the PS principally according to the phase stability, which refers to the small enough $\phi_{N,x,i}$ from all the N interferograms. In order to estimate the $\phi_{N,x,i}$, the PS candidates are firstly selected through the dispersion of amplitude (D_A) (Ferretti et al. 2001). Compared with the classic PS methods, the threshold could be higher to include more PS candidates for the phase stability analysis. For each PSc, an adaptive spatial filter and LAMBDA method (Teunissen 1995) are, respectively, used to eliminate the spatially

correlated components and spatially un-correlated part of look angle error in Eq. (1). It is worthy to note that the spatially correlated components are relatively sensitive to the filtering parameters. For high-resolution images, the filter resample size could be small and the low-pass wavelength should be setting according to priori knowledge on spatial correlation (typical value of 800 m). By removal of the spatially correlated components and un-correlated look angle error from the phase observation, the remaining components in Eq. (1) are expected to be noise and small enough as to have minimum impact on the outcome of the process. Then, the new variable γ_x could be introduced for evaluating the noise level of all the N interferograms,

$$\gamma_x = \frac{1}{N} \left| \sum_{i=1}^{N} exp\left\{ \phi_{x,i} - \widetilde{\phi}_{x,i} - \Delta \widetilde{\phi}_{\varepsilon,x,i}^{u} \right\} \right| \tag{2}$$

where the $\widetilde{\phi}_{x,i}$ and $\Delta \widetilde{\phi}_{\varepsilon,x,i}^{u}$ are, respectively, the sum of four spatially correlated components and estimated spatial un-correlated look angle error. Through four or five times of iterations, with adaptive filtering with different parameters, the optimal γ_x could be retrieved. With the probability density analysis based on both the γ_x and D_A, the PS candidates which are most likely to be stable are kept. By removal of the temporal PSs and adjacent PSs, the final PSs are selected. Once the PS selection finished, the temporal and spatial three- dimensional unwrapping and displacement estimation could be started.

In this study, the steps before PS processing are finished with the Doris software, such as co-registration, interferogram generation, flattening, geocoding, and so on. The DEM from SRTM (Shuttle Radar Topography Mission) on 90-m spatial resolution is introduced to rectify the topographic components in each interferogram. Regarding the height of buildings, the maximum DEM error which is used to control the fitting of spatially uncorrelated look angle error is set to be 15 m. We set the adaptive filtering grid size and unwrap grid size to be 40 and 20 m due to the fact that the resolution of TerraSAR-X images is enough to keep more details and PSs. The maximum PS density is set to be 25 bins per km^2. The unit of the density is bin because the PSs are divided into bins for probability computation, and there are more than 10,000 PSs in each bin. It is necessary to state that the area [22.6745 22.6790N, 113.4735 113.4790E] is selected as the reference area because it is a stable and not subsiding area due to the geological feature of its lithotypes. Meanwhile, this area is close to the GPS reference station, which is more convenient for the comparisons between PSI and GPS results. The PS velocity results are all relative to the mean value of 138 PSs in the reference area. Considering the fact that the monitoring periods in this study is about 18 months, the temporal correlated time window is assigned to be 180 days. The other assignments of the parameters are setting as the suggestions of algorithm.

3 Results and analysis

3.1 PSI results

In the whole area of interest, the selected PSs are 1,27,079, with a density of about 603 PSs per km^2. All coherent values of the PSs are higher than 0.4, and 50.9 % (64,694 PSs) are more than 0.8. The distribution of PSs and the deformation velocity are shown in Fig. 3.
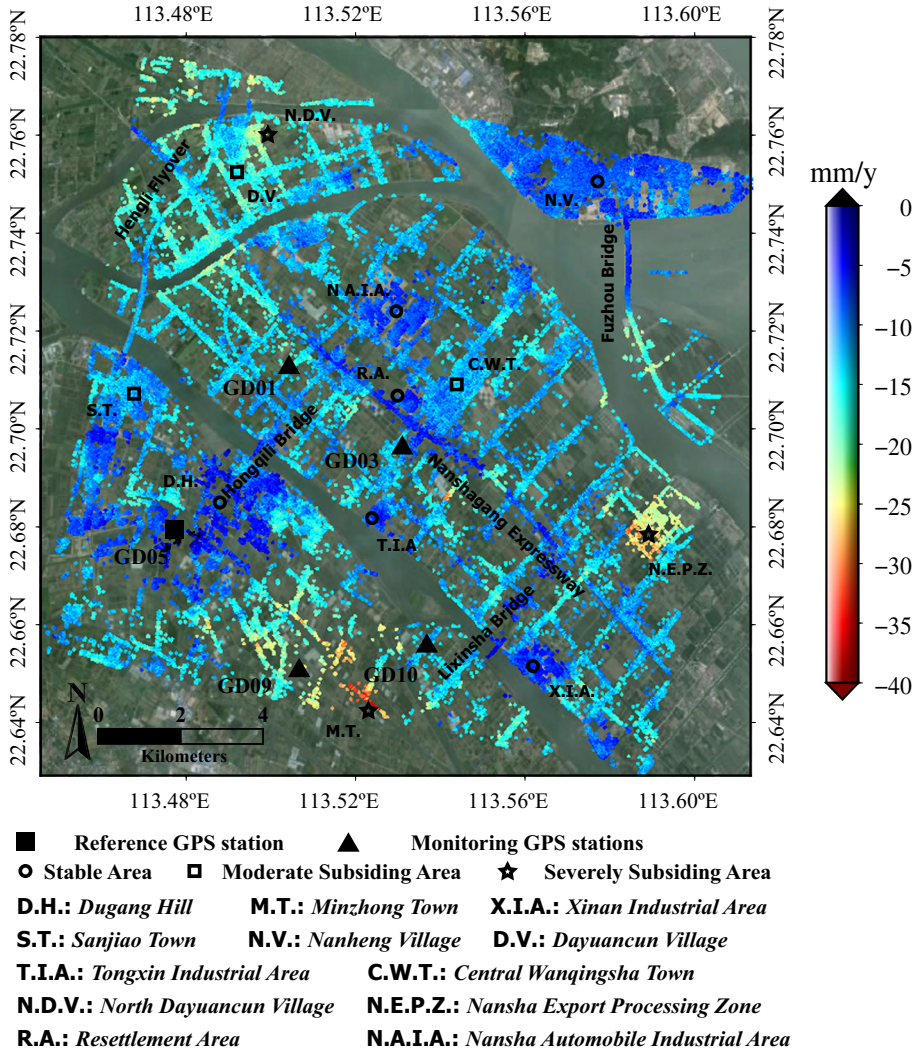
Fig. 3 The distribution and deformation velocity rates of PSs in Nansha District. The base map is the Google image; the *black square* and *triangles* indicate the locations of the reference and monitoring GPS stations. The main built-up areas, roads, and bridges are also shown and listed in notes below

The negative deformation velocity value corresponds to the direction away from the satellite. From Fig. 3, it can be seen clearly that the PSs spatial distribution and density follow the geographic location of built-up areas, roads, and bridges. Concerning the areas covered by radar satellite, the built-up areas include the Wanqingsha town in the center, Nanheng in the right top corner, Hengli in the left top corner, and Zhongshan City in the left bottom. The other PSs cover most of the roads and bridges such as the Nanshagang expressway, which crosses the Wanqingsha town, the Guangao highway connecting the Hengli and Gaoping, the Fuzhou Bridge connecting the Nanheng and Longxuedao Island, the Hongqili bridge, and Lixinsha Bridge on the Hongqili Canal. Regarding the

deformation velocity values, the maximal subsiding and uplifting velocity of the PSs are
−38.47 and 1.96 mm/year; the mean deformation velocity is about −11.42 mm/year. In
detail, the locations of the maximal uplifting points are detected in Dugang in Sanjiao
town. It is worthy to note that the uplifting points might not be true physical uplifting
deformation. It might also caused by the un-removed DEM topographic effects or the
relative deformation in reference area. Contrarily, the maximal subsiding velocity rates
correspond to the areas in the Minzhong town within Zhongshan City.

3.2 Comparison with GPS measurements

In order to validate the PSI results, we introduce the coordinate time series from GPS
measurements for comparison. The GPS results in this study are collected by the "Land
subsidence and geological hazard monitoring of Pearl River delta and its surrounding areas
project". In this project, several GPS stations were constructed for semi-continuous
observation within this region. The locations of 5 GPS stations are shown in Fig. 3 as the
black square and triangles. The measurements started in May 2012 and finished in June
2013. Three of five GPS receivers (GD03, GD05, and GD10) are of dual-frequency, the
remaining two (GD01 and GD09) are single-frequency type. The recording intervals of
GPS receivers are setting to 20 seconds. To facilitate the comparisons, the GPS station
GD05, which is also next to the reference area of PSI processing, is selected as the
reference station during GPS data solutions. The GPS data are processed with the Bernese
5.0 software. During the data processing, the precise IGS final orbits products are intro-
duced. The ocean loading effects are corrected for each station using the ocean tide model.
It is worthy to note that the four deformation time series of GPS stations (GD01, GD09,
GD03 and GD10) are relative to the reference station GD05. The deformation time series
of the 4 GPS stations and the nearby PSs are shown in Fig. 4.

To make a rational comparison between the PSI and GPS results, we select the PSs
based on the following strategies. At first, we determine a central target location. The
selected central pixel location should be next to the GPS station as close as possible and
shares the similar terrain conditions. Once the central pixel location is determined, all the
PSs surrounded within 2 arc-seconds are used to estimate the mean deformation and
standard deviation for the comparison with GPS results. Meanwhile, the deformation time
series from GPS measurements are projected from the NEU coordinates to LOS direction.

It is not difficult to find that there are many PSs around the GPS stations GD01, GD03,
and GD10. The distance values from the selected central pixel location to corresponding
GPS stations (GD01, GD03 and GD10) are, respectively, 30, 50, and 60 m. However, the
station GD09 is located in the crops field, which always exhibits a weak backscattering
characteristic. Thus, the selected central target location is farer away from the GPS station,
which is approximately 120 m. For each PS time series, at least 11 PSs (GD10) are
included for velocity rates estimation. As many as 36 PSs, which are the most of 4 GPS
stations, are introduced for velocity estimation near the GPS station GD03. Due to fact that
most of these nearby PSs share the similar deformation characteristics, the standard
deviation is small. The mean standard deviation of the four time series is about 1.52 mm.

For displacement time series of the GPS stations, the days which were significantly
noisy (with three times of standard deviation) have been removed. It is obvious that the
noise levels of the single-frequency GPS receivers (GD01 and GD09) are much severer
than the dual-frequency receivers (GD03 and GD10). Specifically in the period of June to
August in 2012, the quality of the GPS observations sharply decreases and the deviation
significantly increases to more than 20 m. Such decreasing of observation quality could
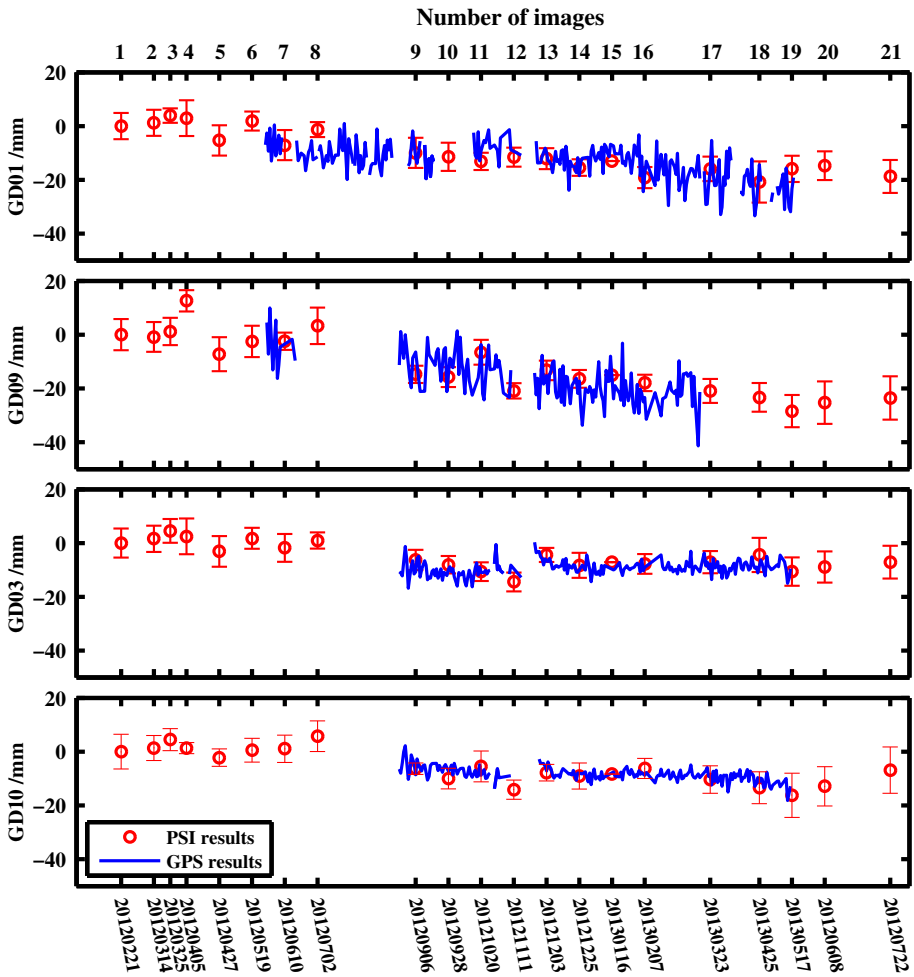
Fig. 4 The LOS deformation time series of PSs and GPS stations. The *cycle* and *curves* are, respectively, the deformations of PSs and GPS stations. The *error bar* of the PSs denotes the three times of standard deviation

also be found in the TerraSAR-X images. For instance, the images acquired on 2012/07/24 and 2012/08/15 are dropped during the solution due to the strong atmospheric effects. The reason for these phenomena might be the extreme weather effects such as typhoons. The weather reports show that there are at least six typhoons (entitled Talim, Doksori, Vicente, Eic, Son Tinh and Bopha) in the referred periods (Wang et al. 2013). Based on the LOS deformation time series, the velocity rates could be retrieved, which is shown in Table 2.

The velocity rates of the GPS and PS are estimated with the linear regression. For the PS velocities, two types of results (corresponding to whole period and period overlapping with GPS measurements) are given. It is clear that during the overlapping periods, the velocity rates between the PS and GPS show a great consistency. The maximum and mean absolute differences between them are the 3.61 and 1.96 mm/year, respectively. Compared with the period overlapping with GPS measurements, the results according to whole period show a weaker

Table 2 The deformation velocity rates from GPS and PSI measurements

GPS station	GPS velocity (mm/year)	PS velocity (mm/year)		
		Overlapping	Period	Whole period
GD01	−14.04	−17.65	6–19 scenes	−16.17
GD09	−26.46	−24.27	6–17scenes	−22.29
GD03	2.21	1.92	9–19 scenes	−8.34
GD10	−7.08	−8.82	9–19 scenes	−11.74

The overlapping period indicates the periods when GPS and PSI measurements are overlapping

consistency. The maximum and mean absolute differences are 10.55 and 5.38 mm/year. It is also observed that the discrepancy between whole and overlapping period results is from February to May 2012, when GPS measurements are unavailable. Among the 4 GPS stations, the most significant discrepancy is shown by GD03. The PS results show that the rapid subsidence gradually stopped when GPS measurements started.

4 Discussion

In whole study area, the subsiding characteristics could be discussed, respectively, on town area, roads, and bridges. It is worthy to note that the discussion is still based on the previous data processing results and by masking the un-correlated nearby points. Therefore, all the subsiding velocities are relative to the reference area mentioned in Sect. 2.

4.1 Subsidence characteristics of the town area

The town area can be approximately divided into three categories according to the subsidence velocity rates in LOS directions from PSI results, the stable area (2 to −5 mm/year), the moderate subsiding area (−5 to −20 mm/year), and the severely subsiding area (more than −20 mm/year). It can be seen in Fig. 3, although the mean subsidence velocity is about −11 mm/year in the study area, there are some places which are stable. The stable areas are Nansha Automobile Industrial Area, the resettlement area in Wanqingsha town, Tongxin Industrial Area and Xinan Industrial Area along the Hongqili Channel, the scientific research area in Nanheng and Dugang of the Gaoping village in Zhongshan City. Nansha Automobile Industrial Area and Tongxin and Xinan Industrial Area finished the construction in 2007. During the planning and construction process, special treatments for soft soil, such as dynamic drainage consolidation, were taken into consideration and implementation. Although the costs of this method are relatively high, it could effectively satisfy the demands of the large industrial areas, storage areas, and building with less floors (Ren et al. 2006). At present, the area is not fully occupied and the existing industrial entities are not of the heavy water drain type. Thus, the load on foundations is relatively small, and the deformation is not significant. The farmer resettlement area was planned and constructed by the government. The construction has been finished in 2006 and experienced its maintenance in 2010. The appropriate planning and continuous maintenance effectively reduce the subsidence phenomenon. For the Nanheng area and Dugang in Gaoping village characterized by lithology, it is expected that these areas will not subside and be stable. Moreover, several maintenance tasks from 2010 to 2011 on the coastal roads ensure the stability.

The moderate subsiding areas with a deformation velocity about −5 to −20 mm/year mainly distribute to the center of Wanqingsha town, Dayuancun village in north of Hengli town, and Gaoping village of Sanjiao town in Zhongshan City. It can be observed in Fig. 1 that these areas are principally the village or town centers with a dense population. Benefit from the rapid development of economy, farmers, and villagers became rich and can afford to decorate and rebuild their houses. Moreover, most of these houses did not take any soft soil foundation treatments. These factors increase the risk of land subsidence. Actually, some of these houses begin to subside or crack even though they appear to be new as is shown in Fig. 5. Figure 5a shows the location of Nianfengcun village, which is in the east of Tongxin Industrial Area. Most area of the Nianfengcun village is suffering of a subsidence velocity about −12 mm/year. A few of them reach a velocity about −20 mm/year. In the Fig. 5b, the level of the road is much lower than the houses due to the land subsidence. The greatest offset distance is even about 18 cm as is shown in Fig. 5d. Meanwhile, because of the asymmetric deformations, the wall of house began to crack gradually in Fig. 5c. As is mentioned in Sect. 2.1, the groundwater in this area is not favorable for life and industrial uses. The residents and enterprises mainly get the water by pumping from the river instead of the underground water. Therefore, the main reason for subsidence is lacking of soft soil foundation treatments.

The severely subsiding areas with subsiding velocity rates higher than −20 mm/year cover Nansha Export Processing Zone in Wanqingsha town, Dayuancun village in the north Hengli town, and Minzhong town in Zhongshan City. Nansha Export Processing Zone was established in 2005. The construction was finished in July 2008, and it is put into operation gradually in late 2009. The deformation maps on LOS direction are shown in Fig. 6.

In Fig. 6, the deformation evolution on both temporal and spatial can be easily found. As the time elapsed, the primary building and the roads in Nansha Export Processing Zone gradually subside. Before July 2012, the deformation maps showed that this area is significantly above the level at reference time (2013/01/16). On the contrary, after March 2013, it is obvious that this area turned out to be below the level at reference time. Among them, the highest and lowest deformations are, respectively, detected in March 2012 and June 2013. During these periods, the mean deformation is 25.97 and −9.52 mm. It can also be found that the deformation maps are not monotonous, but variable. The temporal variation might be introduced by data processing error or real civil constructions. Here we think the cause is likely to be the residual atmospheric error for two reasons. Firstly, the size of the Nansha Export Processing Zone is about 0.91 × 0.91 km^2. And during the data processing, we set the threshold of spatially correlated component with wavelength as 800 m. Considering the fact that the spatially correlated component mainly consists of atmospheric factors, the temporal variation might be caused by residual atmospheric error. Secondly, because the study area is quite close to the sea, the wet weather which changes quickly would easily lead to the unpredictable atmospheric error. Actually, during the data processing, we have dropped two satellite images (2012/07/24 and 2012/08/15) due to the extreme weather such as typhoons. According to its designs (Li 2010), the major traffic in Nansha Export Processing Zone would be heavy trucks. The soft soil foundation processing was adapted to the surcharge pre-compression with vertical drains method to complete the primary consolidation. Then the cement powder was used to constitute the composite foundation to remove the secondary consolidation settlement. Meanwhile, due to the short schedule and planning periods, these procedures have been finished in three months. The subsidence after construction was designed as about 30 cm. It is worthy to
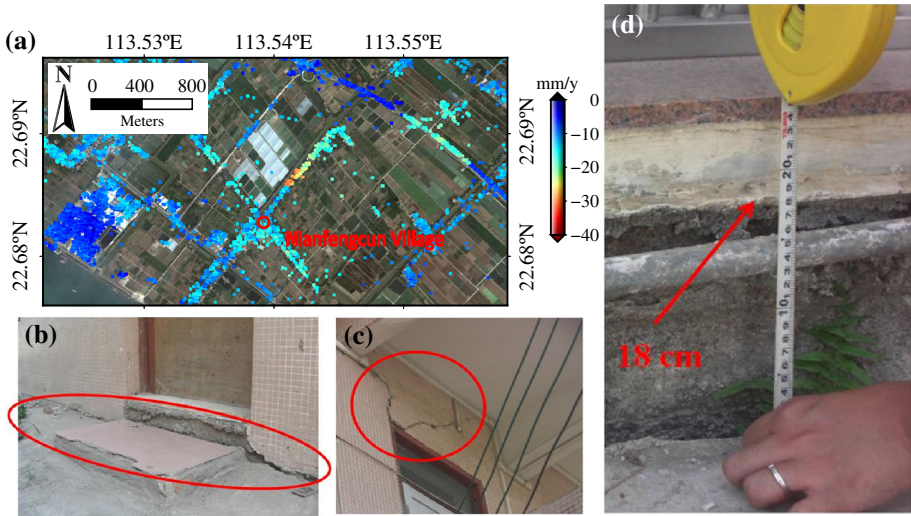
Fig. 5 **a** The location and deformation map from Nianfengcun village. (**b**–**d**) The cracking phenomenon of building caused by land subsidence. The photographs in (**b**–**d**) were taken from different orientations of a house randomly selected in Nianfengcun village
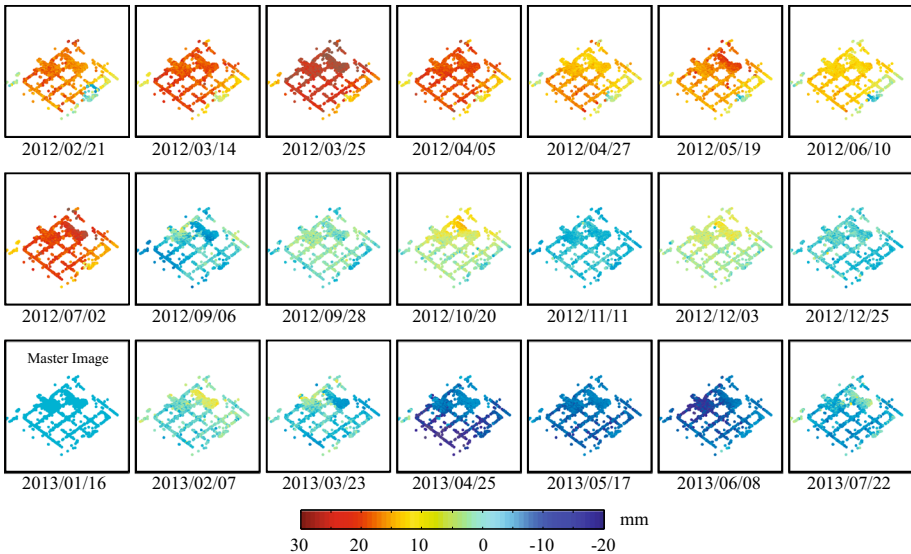

Fig. 6 The deformation maps of the Nansha Export Processing Zone (which is denoted by 'N.E.P.Z' in eastern of the AOI) in Nansha District. The deformation map on 2013/01/16 is the reference map

note that the thickness of soft soil in this district is more than 30 m. Therefore, most of the soft soil foundation processing was difficult to reach the bedrock. This leads to the fact that the post-construction period would last about five years or even more. From the PSI results, the subsiding velocity in this area is about −25 mm/year, which is approximately

consistent with the post-construction subsidence designs and indicating that it is in the normal subsiding period.

In Dayuancun village of the north Hengli, there are so many self-built houses of the nearby farmers. Most of these self-built houses did not take any soft soil foundation treatment, which leads to the severe subsidence. Minzhong is one of the largest towns in northeastern Zhongshan City. In the past years, the Minzhong town has suffered from many kinds of geological hazards besides the land subsidence, such as the collapse, landslide, and debris flow induced by the hilly terrain and extreme weather as typhoon and precipitations (Lin 2010). Too much attention and resources from the local government and villagers were allocated on the prevention or control of hazards, which is not accumulative and imperceptible as subsidence. Like north Dayuancun village, most of the building and houses here have not taken any soft soil foundation treatments. In recent years, phenomena as the cracks on houses, walls, and roads caused by the land subsidence are gradually manifested. Fortunately, these phenomena have attracted the attention from Zhongshan City government. Several places have been listed as the key prevention areas in the Geological Hazards Control Programming published by government of Zhongshan City (http://www.zsfdc.gov.cn/Article.aspx?id=833).

4.2 Subsidence characteristics of primary roads and bridges

Despite the town areas, the subsidence of roads and bridges is also noteworthy (Cao 2003). Several main roads and bridges such as Hengli Flyover, Fuzhou Bridge, Nanshagang Expressway, Hongqili, and Lixinsha bridges in study area are shown in Fig. 7.

The Hengli Flyover is located in the central Hengli town, between the Shanghengli and Xiahengli Channels. As shown in Fig. 7a, it is the intersection of the Beijing-Zhuhai Highway (from northeast to southwest) and Nanshagang Expressway (from northwest to southeast). It completed the first and second periods of designs and constructions in 2005 and 2008, respectively. In the April, 2011, it is gradually open to the traffics. During the two periods of treatments on soft soil roads foundations, the surcharge pre-compression with vertical drains method and composite roadbed were, respectively, introduced. The benefits of these treatments are of short periods, prone to the strict control of post-constructions, and especially suitable for small soft soil particles geological environments. The post-construction subsiding displacement of the Hengli Flyover was designed to be 20 cm. According to the PSI results in this study, the general subsiding velocity is about −15 mm/year. Moreover, it can be seen that the average velocity of Beijing-Zhuhai Highway is slightly larger than the Nanshagang Expressway. The local investigation results show that the project Beijing-Zhuhai Highway is finished later than Nanshagang Expressway. Thus, they are experiencing the different subsiding periods. This is the main reason for the difference on subsiding velocity. As shown in Fig. 7a, the different part of the roads might be also subsiding with different velocities. Actually, there are two reasons. The first one is due to the different construction schedule as mentioned above. The second reason is because the nearby houses. For instance, the points with subsiding velocity more than −15 mm/year at the west of the intersections of flyover are from the residential houses. Some of these dense houses which are too close to the roads are not easy to be totally separated from the roads in remote sensing images. In other words, the flyover is still likely to be experiencing the subsiding periods controlled by designs as the Nansha Export Processing Zone mentioned above.

The Fuzhou Bridge, which connects the Nanheng and Longxuedao Island as shown in Fig. 7b, was open to public in August 2008. Compared with the stable geological
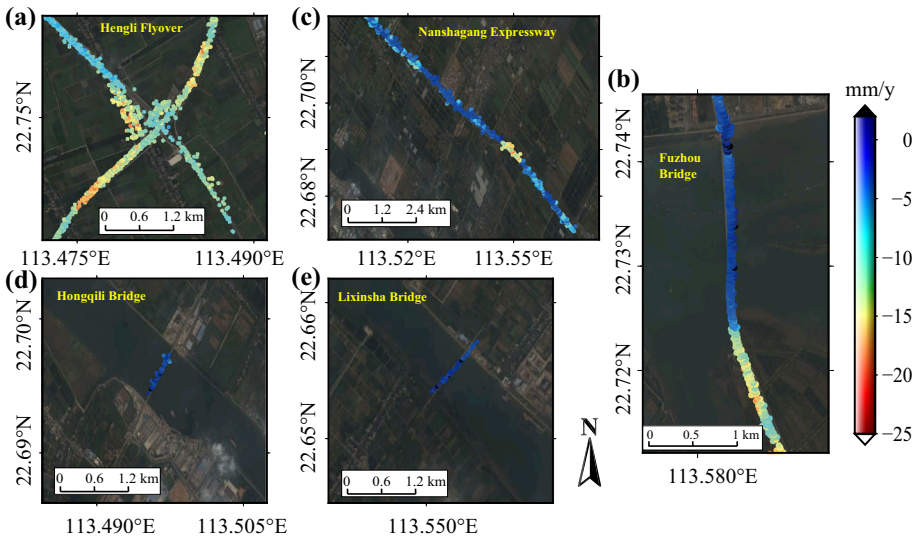
Fig. 7 **a** Subsiding velocity of Hengli Flyover, **b** Subsiding velocity of Fuzhou Bridge, **c** Subsiding velocity of Nanshanggang Expressway, **d** Subsiding velocity of Hongqili Bridge, **e** Subsiding velocity of Lixinsha Bridge

environments on the north side, the treatments for soft soil of roadbed on south side is worthy to discuss moreover. On the south side, the combined vacuum and surcharge pre-compression method was adopted. The mud mixing, vacuuming, blown sanding, and other technologies were implemented in order. The subsiding displacement was designed to be 10 cm after construction. The average velocity rates from the PSI results are about −15 mm/year, indicating that the subsidence is well within the design specification during the post-construction settling phase. It is likely that the subsidence will continue before reaching to a stable state. For the bridge body, the PSI results show that it is relatively stable. But from the Fig. 7b, the mm level difference on deformation velocity can also be found in different parts of the bridge body. Different from the roads, the velocity variation of bridge is much smoother and smaller. The changes of velocity are not likely to be the different construction schedule. One possible reason might be the self-deformations or vibrations due to temperature variation, traffic, or wind loads.

The Nanshagang Expressway, which is throughout the whole Nansha District as shown in Fig. 7c, was put into use in 2005. Except the section next to the Hengli Flyover mentioned above, most sections have experienced the subsiding periods and access the stable state. The stable state is obviously reflected in the PSI results, which is almost of no subsiding velocity. It is worthy to note that there is a subsiding location at about [N22.69, E113.55]. The local investigation results show that it just has finished the repairing and maintenance. This is the most possible reason for the land subsidence.

It can be found in Fig. 7d, e that the Hongqili and Lixinsha are two most important bridges over the Hongqili Channel. The PSI results show that they are quite stable without significant subsiding velocity. This is expected since these two bridges were built in the 80 and 90s in twenty century. With several times of maintenance, they have finished the subsiding periods and been stable.

5 Conclusion

In this study, a specially designed StaMPS/MTI procedure is employed using 21 high-resolution TerraSAR-X satellite images to recover the subsidence features of the target region. The specially designed processing strategy is proven to be very effective. The comparison between the PSI and GPS results shows a favorable agreement. For the four GPS stations and the corresponding PSI results, the maximum and mean absolute differences between them are, respectively, 3.61 and 1.96 mm/year. The PSI results show that most of the stable areas are located on the Nansha Automobile Industrial Area, Tongxin Industrial Area, Xinan Industrial Area, Nanheng, and Dugang of Sanjiao town in Zhongshan City. The areas with moderate subsidence are mainly spared over the Dayu-ancun village and Gaoping village of Sanjiao town in Zhongshan City. The areas under-going severe subsidence are detected in the Nansha Export Processing Zone and Minzhong town in Zhongshan City. For primary roads and bridges, the lately built bridges, such as Hengli Flyover and southern side of Fuzhou Bridges, are suffering a subsidence velocity range from −10 to −15 mm/year. In contrast, the older ones turned out to be stable, for instance, the Nanshagang Expressway, Hongqili, and Lixinsha Bridges. The subsidence rates obtained from this study indicate that they are as expected during the post-construction settling phase as specified by the engineering design. Some of the self-constructed houses in the region suffered varying degree of structural damage from the subsidence in certain areas due to lack of proper construction of the foundation required for soft soil condition. From the aspects of data process, both the parts of SAR and GPS observations were subject to the extreme weather such as typhoons. By collecting more TerraSAR-X images and higher-resolution DEM data, longer and more precise deformation monitoring results can be realized in future.

References

Amelung F, Galloway DL, Bell JW et al (1999) Sensing the ups and downs of Las Vegas: InSAR reveals structural control of land subsidence and aquifer-system deformation. Geol 27(6):483–486
Bawden GW, Thatcher W, Stein RS et al (2001) Tectonic contraction across Los Angeles after removal of groundwater pumping effects. Nat 412(6849):812–815
Bianchini S, Cigna F, Del Ventisette C et al. (2012) Detecting and monitoring landslide phenomena with TerraSAR-X persistent scatterers data: The Gimigliano case study in Calabria Region (Italy). IEEE Int Geosci and Remote Sens Symp (IGARSS) Munich:982–985.
Bianchini S, Cigna F, Del Ventisette C et al (2013) Monitoring landslide-induced displacements with TerraSAR-X persistent scatterer interferometry (PSI): Gimigliano case study in Calabria region (Italy). Int J Geosci 4(10):1467–1482
Cabral-Cano E, Dixon TH, Miralles-Wilhelm F et al (2008) Space geodetic imaging of rapid ground subsidence in Mexico City. Geol Soc Am Bull 120(11–12):1556–1566
Cao X et al (2003) Analyses and approach to treatment option of subgrade soft soil foundation in Nansha area. Urban Roads Bridges Flood Control 6:30–32
Chang CP, Yen JY, Hooper A et al (2010) Monitoring of surface deformation in Northern Taiwan using DInSAR and PSInSAR techniques. Terr Atmos Ocean Sci 21(3):447–461

Chen B, Gong H, Li X et al (2011) Spatial-temporal characteristics of land subsidence corresponding to dynamic groundwater funnel in Beijing municipality, China. Chin Geogra Sci 21(6):753–763

Chen J, Wu J, Zhang L et al (2013) Deformation trend extraction based on multi-temporal InSAR in Shanghai. Remote Sens 5(4):1774–1786

Chen W, Zhao H, Chang Y et al (2001) The rate of late quaternary vertical motion of the Zhujiang delta. Seismolog Geol 23(2):527–536

Cigna F, Del Ventisseti C, Liguoli V et al (2011) Advanced radar-interpretation of InSAR time series for mapping and characterization of geological processes. Nat Hazards Earth Syst Sci 11(3):865–881

Cigna F, Osmanoğlu B, Cabral-Cano E et al (2012) Monitoring land subsidence and its geological hazard with Synthetic Aperture Radar: a case study in Morelia, Mexico. Remote Sens Environ 117:146–161

Ferretti A, Fumagalli A, Novali F et al (2011) A new algorithm for processing interferometric data-stacks: SqueeSAR. IEEE Trans Geosci Remote Sens 49(9):3460–3470

Ferretti A, Prati C, Rocca F (2000) Non-linear subsidence rate estimation using permanent scatterers in differential SAR interferometry. IEEE Trans Geosci Remote Sens 38(5):2202–2212

Ferretti A, Prati C, Rocca F (2001) Permanent scatterers in SAR interferometry. IEEE Trans Geosci Remote Sens 39(1):8–20

Finnegan NL, Pritchard ME, Lohman RB et al (2008) Constraints on surface deformation in the Seattle, WA, urban corridor from satellite radar interferometry time-series analysis. Geophys J Int 174(1):29–41

Gens R, Van Genderen JL (1996) Review article SAR interferometry−issues, techniques, applications. Int J Remote Sens 17(10):1803–1835

Heleno SIN, Oliveira LGS, Henriques MJ et al (2011) Persistent Scatterers Interferometry detects and measures ground subsidence in Lisbon. Remote Sens Environ 115(8):2152–2167

Hoffmann J, Zebker HA, Galloway DL et al (2001) Seasonal subsidence and rebound in Las Vegas Valley, Nevada, observed by synthetic aperture radar interferometry. Water Resour Res 37(6):1551–1566

Hooper A (2008) A multi-temporal InSAR method incorporating both persistent scatterer and small baseline approaches. Geophys Res Lett 35(16):L16302

Hooper A, Segall P, Zebker H (2007) Persistent scatterer interferometric synthetic aperture radar for crustal deformation analysis, with application to Volcán Alcedo. Galápagos. J Geophys Res: Sol Ea 112(B7):B07407

Hooper A, Zebker H, Segall P et al (2004) A new method for measuring deformation on volcanoes and other natural terrains using InSAR persistent scatterers. Geophys Res Lett 31(23):L23611

Kampes B (2006) The Permanent Scatter Technique, In Radar interferometry: Persistent scatterer technique. Springer, Dordrecht, Netherlands

Li C (2010) Generalization of road design in Guangdong Nansha export processing zones. Shanxi Archit 36(16):259–260

Lin L (2010) Discussion on the geological environment and geological disasters characteristics in Zhong-shan city of Guangdong. Shanxi Archit 36(7):97–98

López-Quiroz P, Doin MP, Tupin F et al (2009) Time series analysis of Mexico City subsidence constrained by radar interferometry. J Appl Geophys 69(1):1–15

Lubitz C, Motagh M, Wetzel HU et al (2011) Remarkable Urban uplift in Staufen im Breisgau, Germany: observations from TerraSAR-X InSAR and leveling from 2008 to 2011. Remote Sens 5(6):3082–3100

Massonnet D, Feigl KL (1998) Radar interferometry and its application to changes in the earth's surface. Rev Geophys 36(4):441–500

Milan L, Eva J (2010) Longtime monitoring of mine subsidence in Northern Moravia, Czech republic using different insar techniques. IEEE International Geoscience and Remote Sensing Symposium (IGARSS), 2010 IEEE International, pp 3331–3334

Motagh M, Wetzel HU, Roessner H et al (2013) A TerraSAR-X InSAR study of landslides in southern Kyrgyzstan, Central Asia. Remote Sens Lett 4(7):657–666

Ouchi K (2013) Recent trend and advance of Synthetic Aperture Radar with selected topics. Remote Sens 5(2):716–807

Perissin D, Wang T (2011) Time-Series InSAR applications over urban areas in China. IEEE J Select Topics Appl Earth Observ Remote Sens 4(1):92–100

Ren Y, Zeng W, Peng S et al (2006) Eco-industrial network design of the international automobile industrial area in Nansha. Yunnan Environ Sci 25(3):11–14

Schmullius CC, Evans DL (1997) Review article Synthetic aperture radar (SAR) frequency and polarization requirements for applications in ecology, geology, hydrology, and oceanography: A tabular status quo after SIR-C/X-SAR. Int J Remote Sens 18(3):2713–2722

Song F, Wang Y, Li C et al (2003) Late quaternary vertical dislocation rate on several faults in the Zhujiang delta area. Seismolog Geol 25(2):203–210

Teunissen P (1995) The least-squares ambiguity decorrelation adjustment: a method for fast GPS integer ambiguity estimation. J Geodesy 70(1–2):65–82

Wang Y, Ye D, Ai W et al (2013) Climatic characteristics over China in 2012. Meteorol Mon 39(4):500–507

Wang Z, Liu H (2011) Hydrogeological characteristics and aquifer structural analysis on southern Guangzhou. Ground Water 33(4):79–81

Wegmuller U, Walter D, Spreckels V et al (2010) Nonuniform ground motion monitoring with TerraSAR-X persistent scatterer Interferometry. IEEE Trans Geosci Remote Sens 48(2):895–904

Wu T, Yang M, Li Y (2011) Assessment of Groundwater Specific Vulnerability In Guangzhou Based On Fuzzy Comprehensive Evaluation. International Symposium on Water Resource and Environmental Protection (ISWREP) 25:798–804

Xu R, Li W, Wang K (2009) Hydrology sediment condition and sedimentation analysis of Nansha Port, Guangzhou. Port Waterway Eng 429(7):29–35

Yao Y, Zhan W, Liu Z et al (2008) Neotectonics of the pear river delta and its relationship with the deltaic evolution. South China J Seismolog 28(1):29–40

Zhang L, Lu Z, Ding X et al (2012) Mapping ground surface deformation using temporarily coherent point SAR interferometry: application to Los Angeles Basin. Remote Sens Environ 117:429–439

Zheng J, Liu R (2006) Types and characters of groundwater in Guangzhou area and its affection to city construction environment. Trop Geogr 26(3):264–268